The Human Papillomavirus E7−E2 Interaction Mechanism in Vitro Reveals a Finely Tuned System for Modulating Available E7 and E2 Proteins[†]

Clara Smal,[‡,§] Diana E. Wetzler,[‡,§] Karina I. Dantur,[‡] Lucia B. Chemes,[‡] María M. Garcia-Alai,[‡,⊥] Mariano Dellarole,[‡] Leonardo G. Alonso,[‡] Kevin Gaston,[∥] and Gonzalo de Prat-Gay*,[‡]

[‡]*Fundación Instituto Leloir and Instituto de Investigaciones Bioquímicas, CONICET, Patricias Argentinas 435, 1405 Buenos Aires, Argentina,* [§]*Facultad de Ciencias Exactas y Naturales, Universidad de Buenos Aires, Buenos Aires, Argentina, and* [∥]*Department of Biochemistry, School of Medical Sciences, University of Bristol, Bristol BS8 1TD, United Kingdom.* [⊥]*Present address: Medical Research Council Centre for Protein Engineering, Cambridge CB2 0QH, United Kingdom.*

ABSTRACT: Transcription of the human papillomavirus E7 oncoprotein is negatively controlled by the viral E2 protein, and loss of this repression leads to irreversible transformation and carcinogenesis. Here we show that interaction of the HPV16 E7 protein with the DNA binding domain of the E2 protein (E2C) leads to ionic strength-dependent hetero-oligomerization even at the lowest concentrations measurable. Titration experiments followed by light scattering and native gel electrophoresis show insoluble oligomeric complexes with a ≥2000 nm diameter and intermediate soluble complexes 40 and 115 nm in diameter, respectively, formed in excess of E2C. A discrete oligomeric soluble complex formed in excess of E7 displays a diameter of 12 nm. The N-terminal domain of E7 interacts with E2C with a K_D of 0.1 μM, where the stretch of residues 25−40 of E7, encompassing both a PEST motif and phosphorylation sites, is sufficient for the interaction. Displacement of the soluble E7−E2C complex by an E2 site DNA duplex and site-directed mutagenesis indicate that the protein−protein interface involves the DNA binding helix of E2. The formation of complexes of different sizes and properties in excess of either of the viral proteins reveals a finely tuned mechanism that could regulate the intracellular levels of both proteins as infection and transformation progress. Sequestering E2 into E7−E2 oligomers provides a possible additional route to uncontrolled E7 expression, in addition and prior to the disruption of the E2 gene during viral integration into the host genome.

Most of the adult worldwide population is exposed to different types of human papillomavirus (HPV) that cause mucosal or skin lesions, which can either resolve spontaneously or progress into benign or malignant tumors (*1*). HPVs infect epithelial cells, and the viral life cycle is intimately linked to the proliferation and differentiation of these cells. The viral proteins that interfere with the normal cellular controls that regulate these events can act as oncoproteins. Cervical cancer is the most statistically significant threat associated with HPV types, where 80% of these cancers occur in developing countries (*2*). Effective vaccines have been developed for preventing infection by certain types of HPVs, whereas therapeutic vaccines for treating HPV-induced cancer have not yet reached the market. However, it is estimated that 5 million cancer deaths will occur over the next 20 years due to existing HPV infections (*3*).

Eight proteins are encoded in the small 8 kb circular DNA genome of HPVs; two of them, E6 and E7, cooperate during cell transformation by the virus (*4*). The primary event behind transformation by E6 is binding and degradation of p53 (*5*). On the other hand, E7 binds the retinoblastoma (pRb) tumor suppressor (*4*), promoting its degradation via the ubiquitin proteasome system (*6*). E7 counterparts in other DNA tumor viruses such as E1A from adenovirus and large T-antigen in SV40 also bind to pRb, thus validating a common viral strategy (*7*). E7 is the major transforming protein in HPV, since its interaction with hypophosphorylated pRb causes disruption of growth-suppressive pRb−E2F complexes. These complexes play important roles in the regulation of the G1/S phase transition by promoting DNA replicative conditions required for replication of the viral genome (*5, 6*). A wide variety of binding partners of E7 have been and continue to be identified by different methods, suggesting multiple ways by which E7 may induce transformation and subsequent progression into cancer. E7 has a relatively short half-life in HPV-transformed CaSki cells, and its degradation, both in vitro and in vivo, is mediated by the ubiquitin−proteasome pathway (*8*). E7 also has an N-terminal region harboring a CKII consensus site responsible for the phosphorylation of two serine residues (S31 and S32). This region, rich in acidic amino acids, includes a PEST sequence (*9*), and mutagenesis studies suggested that it is involved in the regulation of E7 stability (*10*). The fact that PEST sequences have been shown to regulate the stability of short-lived proteins (*11*) suggests that the same may be true for E7. Phosphorylation of a PEST sequence in BPV E2 was shown to alter the local thermodynamic stability and half-life within cells (*12*).

*To whom correspondence should be addressed: Fundación Instituto Leloir and Instituto de Investigaciones Bioquímicas, CONICET, Patricias Argentinas 435, 1405 Buenos Aires, Argentina. Phone: 54-11-5238-7500. Fax: 54-11-5238-7501. E-mail: gpg@leloir.org.ar.

Despite the small size of E7 (98 residues), a large number of different protein targets have been described, making its particular conformational properties puzzling. HPV16 E7 is an extended dimer in solution with pH-dependent conformational transitions leading to differential levels of exposure of hydrophobic surfaces, which we proposed could be related to its ability to bind different proteins (*13*). HPV16 E7 can self-assemble into soluble and highly stable spherical oligomers (E7SOs) 50 nm in diameter and 790 kDa in mass (*14*) which display chaperone holdase activity for model chaperone substrate proteins at substoichiometric concentrations (*15*). These oligomers exhibit amyloid-like properties, as judged by their ability to bind Congo Red and thioflavin-T (*14*). This is consistent with the formation of a molecular scaffold that allows multiple binding partners to bind simultaneously to an E7 assembly in vivo (*16*).

Structures of two E7 proteins (from HPV45 and HPV1a) have been determined by NMR and X-ray crystallography, respectively, and revealed a highly dynamic N-terminal domain in solution and a C-terminal globular and well-structured zinc-binding domain with a $\beta 1\beta 2\alpha 1\beta 3\alpha 2$ topology (*17*, *18*). The N-terminal domain of HPV16 E7 is intrinsically disordered, and although it is neither compact nor cooperatively folded, it is a bona fide functional domain that has probably evolved to maintain a dynamic but extended structure in the cell (*19*). These properties would provide adaptability for binding to a variety of protein targets through this domain.

E2 is the master regulator of the virus life cycle, where its main roles involve the control of gene transcription and viral genome replication (*20*, *21*). E2 acts as a loading factor for the viral E1 helicase at the HPV origin of replication. E2 can also repress transcription of integrated genomes, although it does not appear to repress transcription from HPV episomes (*22*). The gene silencing effect of E2 was shown to depend on interaction with the Brd4 domain (*23*). An additional important function relates to migration of the viral episome where E2 acts to tether HPV DNA to mitotic chromosomes to ensure equal segregation, mediated by the interaction of E2C with Brd4 (*24*). Many cellular and viral proteins have been shown to interact with E2 (*21*, *25*). The E2 proteins are ca. 400 amino acid polypeptides consisting of an N-terminal transactivation domain (ca. 200 amino acids) and a C-terminal DNA binding and dimerization domain (E2C, ca. 85 amino acids), separated by a nonconserved "hinge" domain. E2C domains from all strains analyzed so far share a particular folding topology, the dimeric β-barrel (*26*).

Carcinogenesis by HPV appears to require integration of viral DNA into the host cell genome, and there is a correlation between the progress of the cancerous lesion and integration (*27*). The E2 open reading frame is almost always disrupted upon integration (*28*), and the consequent loss of E2 repression of E6 and E7 transcription results in enhanced proliferation and genetic instability (*29*). However, E2 can suppress transcription from integrated genomes and not from HPV episomes. A direct interaction between E2 and E7 was reported in vivo, where E2 was capable of inhibiting E7-ras cooperation in cell transformation and showed a marked effect on E7 stability and localization (*30*, *31*). In this work, we set out to dissect the biochemical interaction mechanism between the HPV16 E7 oncoprotein and E2. We found that the DNA binding domain of E2 (E2C) interacts in solution with E7 and determined that the folded structure of this E2 domain is required for tight interaction. We characterized the complexes formed at different concentration regimes that could be representative of different stages of the

infection and cell differentiation processes. Finally, accurate quantitative methods allowed us to map the interaction site of each protein, and we postulate a plausible model to explain the fine regulation of E2 and E7 protein levels and their roles in the control of cell proliferation.

EXPERIMENTAL PROCEDURES

Reagents. Recombinant E7 HPV16 protein (100 amino acids) was expressed and purified as previously described (*13*). High-molecular weight E7 oligomers, E7SOs, were obtained as described previously (*14*). E2C HPV16 (81 amino acids) and mutants were produced, as described previously (*32*).

E7 peptides corresponding to the N-terminus of E7 HPV16 and the α1-E2C peptide were obtained from the Keck facility (Yale University, New Haven, CT), purified by reverse phase HPLC, and submitted to mass spectrometry. The peptides were dissolved in water (pH 8.0), and quantification was conducted by absorbance at 276 and 220 nm in HCl. The α1-E2C peptide contains residues 289−307 of HPV16 E2 (LKGDANTLK-CLRYRFKKHA). The last residue in the sequence was mutated from Cys to Ala to avoid redox side reactions.

Double-stranded 18 bp oligonucleotides containing the E2 recognition sequence (position 35 in the HPV16 genome) were prepared as follows. Single-stranded oligonucleotides were purchased, HPLC-purified, from Integrated DNA Technologies. We annealing the oligonucleotides by mixing equal amounts in 10 mM Bis-Tris-HCl buffer (pH 7.0) and 50 mM NaCl, incubating the samples for 5 min at 95 °C, and further slowly cooling them to 25 °C for 16 h.

E7 HPV16 and synthetic peptides were labeled with fluorescein isothiocyanate (FITC, Sigma catalog no. F-3651). The coupling reaction was conducted via addition of 1.5 mg/mL FITC to 1 mg/mL full-length E7 or E7 peptides in 50 mM carbonate buffer (pH 10.0 or 8.0, respectively) and 1 mM DTT for 3 h at room temperature. The reactions were stopped with 50 mM Tris-HCl (pH 8.0), and nonlabeled FITC was subsequently removed by size exclusion chromatography in a PD10 column (General Electric) in 50 mM Tris-HCl (pH 8.0) and 1 mM DTT. Full-length E7, E7N [E7(1−40)], E7(16−40), and E7 BPV peptide, all samples labeled with FITC, were purified by filtration in Superdex 75 (General Electric). Labeled E7(25−40), E7(16−31), and E7(1−20) were purified by reverse phase HPLC. All labeled samples were tested via mass spectrometry. Protein concentrations were determined by the Bradford colorimetric assay, and concentrations of FITC-labeled E7 peptides were determined from absorbance measurements at 492 nm.

Cell Lines, Electrophoretic Methods, and Immunodetection.   (*i*) *EMSA*. Samples were incubated at an E7:E2C concentration ratio equal to 1 in 100 mM NaCl, 20 mM Tris-HCl (pH 8.0), and 2 mM DTT. When the E2C−E7N interaction was assayed, samples were incubated with 20 μM E7N and an increased concentration of E2C under the same conditions used for titration curves. Mixtures were loaded in a 6% polyacrylamide native gel containing 2% glycerol, 25 mM Tris-HCl (pH 8.3), 190 mM glycine, and 2 mM DTT. The native gels were stained with Coomasie blue.

(*ii*) *Cell Culture*. CaSki cells derived from HPV16-positive human cervical cancer (*33*) and non-HPV human osteosarcoma cell line U2-OS were purchased from the American Type Culture Collection (ATCC). CaSki cells were maintained in RPMI medium1640 (GIBCO, Invitrogen) with 10% FBS; U2-OS cells were grown in McCoy's medium (GIBCO, Invitrogen) with 10% FBS.

(*a*) *Western Blotting*. Cells ($\sim$5 $\times$ 10^6) were lysed for 30 min in ice-cold CHAPS buffer (1% CHAPS in PBS, 2 mM MgCl$_2$, 50 μM MG132, 2 mM DTT, 2 mM PMSF, and protease inhibitor cocktail from Sigma). Whole cell extracts were centrifuged at low speed, and the nuclear pellet was resuspended in the same lysis buffer and sonicated for 5 s. After centrifugation at maximal speed, the second fraction was pooled with the first one and the total protein content was determined by Bradford quantification assay. Five or ten micrograms of whole cell lysates and 10 ng of recombinant and purified HPV16 E7 or HPV16 E2C were separated on a 15% SDS−polyacrylamide gel and transferred to a Hybond polyvinylidene difluoride (PVDF) membrane (Amersham Bioscience). Membranes were blocked in 3% BSA in Tris buffer saline (TBS) overnight at 4 °C and subsequently incubated for 1.5 h at RT with the anti-E7 monoclonal M1 antibody (1:500 dilution in 0.25% BSA/TBS and 0.1% Tween 20). An HRP-conjugated anti-mouse IgG secondary antibody was used, and the membranes were analyzed with an enhanced chemiluminescence detection plus system (ECLplus, Amersham).

(*b*) *Far Western Blot*. Purified recombinat proteins HPV16 E7 and HPV16 E2C and CaSki and U2-OS lysate samples were separated by SDS−PAGE and transferred to a PVDF membrane. The membrane was blocked with 2% BSA in TBS ON at 4 °C, washed, and subsequently probed on-membrane with 5 μg/mL purified E2C [diluted in 25 mM Tris-HCl (pH 7.5), 0.25% BSA, and 0.05% Tween 20] for 2 h at RT. After the samples had been extensively washed, bound E2C was detected by incubating the membrane with a mouse anti-E2 monoclonal antibody (*34*). The proteins corresponding to bands were visualized after incubation with an HRP-conjugated anti-mouse IgG secondary antibody and with the enhanced chemiluminescence detection plus system (ECLplus, Amersham).

Light Scattering Measurements. Absorbance scattering measurements were taken using a Beckman Coulter DTX 880 multimode detector and a Bio-Rad 550 microplate reader (340 and 415 nm, respectively). All the conditions were measured in 96-well plates (Corning nonbinding surface). Complex protein aggregation kinetics were recorded in a Jasco UV spectrophotometer by following scattering signals at 360 nm immediately after both proteins had been mixed. Measurements were performed in 20 mM Tris-HCl (pH 8.0) and 1 mM DTT.

Measurements were conducted in different tubes containing the same E2C concentration (2 μM) and varying E7 concentrations in the presence of 20 mM Tris-HCl (pH 8.0) and 1 mM DTT. Protein mixtures were incubated for 5 min until they reached the steady state after scattering signals had been recorded at 360 nm in a Jasco UV spectrophotometer. The 280 nm absorbance of soluble fractions was measured after centrifugation of the samples. This was done in the same apparatus. Then the pellet fraction and soluble fraction-precipitated TCA were analyzed via SDS−PAGE.

DLS measurements were taken on a Zetasizer Nano S DLS device from Malvern Instruments (Malvern). Measurements were taken in 20 mM Tris-HCl (pH 8.0) and 1 mM DTT at 20 °C. E7 and E2C were filtered with Ultrafree-MC microcentrifuge filters (0.22 μm, Millipore) before measurements were taken. Protein mixtures were measured before and after centrifugation.

In constrained analysis, analysis of the data was conducted by constraining the particle size range to specific limits. In E7 excess experiments, the analysis was performed between 20 nm and 1 μm. Under stoichiometric conditions or in an excess of E2C, the analysis was constrained to a 0.1−20 nm range.

Fluorescence and Circular Dichroism Spectroscopy. Fluorescence anisotropy titration measurements and fluorescence intensity measurements were conducted using an Aminco-Bowman Series 2 spectrofluorimeter. The fluorescein-labeled protein or peptide was diluted to the desired concentration. The assay buffer consisted of 20 mM Tris-HCl (pH 8), 50 mM NaCl, and 5 mM DTT. The E2C protein was diluted appropriately in stepwise dilutions. The total volume reached less than 10% in each assay, and thus, the concentration of E7 protein or E7 peptides can be assumed to have remained constant. Parallel and perpendicular emission components were measured in L-format by excitation at 495 nm and emission at 520 nm. Anisotropy and fluorescence intensity were measured five times at each titration point with an integration time of 3 s for each intensity measurement, and the resulting anisotropy values were averaged. The standard deviation for fluorescence anisotropy measurements was in the range of ±0.0003. A similar protocol was used to titrate FITC-E7N with the α1-E2C peptide.

The dissociation constant (K_D) of the complex was calculated by fitting the plot of observed fluorescence anisotropy (*r*) change of E7 or E7 peptides versus added E2C to the following equation assuming a 1:1 stoichiometry (*35*):

$$r = r_{\text{free}} + \frac{\Delta r_{\text{int}}}{2} \left\{ (x + [\text{E7}] + K_D) - [(x + [\text{E7}] + K_D)^2 - 4[\text{E7}]x]^{0.5} \right\} \quad (1)$$

where *x* is the variable total concentration of E2C, Δr_{int} is the difference in intrinsic fluorescence anisotropy between the free and complexed fragments, and r_{free} is the fluorescence anisotropy of the free fragment. In the cases in which the fluorescence intensity changed more than 15% during titration curves, the fraction bound was calculated in each point according to the method of Lakowicz (*36*). The initial and final fluorescence intensity and anisotropy values needed to fit parameters were measured under saturated conditions (data not shown).

Far-UV CD measurements were conducted on a Jasco J-810 spectropolarimeter using a Peltier temperature-controlled sample holder and a 0.1 cm path length cell. All samples were incubated for 5 min until reaching the steady state in 20 mM Tris-HCl (pH 8.0) and 1 mM DTT at 20 °C.

RESULTS

Interaction between HPV16 E7 and the E2C Domain. On the basis of our own preliminary experiments in which an E7−E2C mixture showed a tendency to aggregate at low concentrations, we looked for physical evidence of a direct interaction between recombinant E7 and E2C from HPV16 starting with an electrophoretic mobility shift assay [EMSA (Figure 1A)]. E2C does not enter the native gel because of its high basic pI (9.8), whereas the E2C−E7 complex runs retarded compared to E7. The shape of the E2C−E7 band suggests that the electrophoretic conditions are dissociative.

To investigate the binding of E2C to recombinant or endogenous E7 from HPV-transformed cells, we performed far Western experiments. We analyzed whole cell lysates from the HPV16-transformed CaSki cells and non-HPV-transformed U2-OS cells. Total extracted proteins were separated by SDS−PAGE, and E7 was detected by Western blotting using the anti-HPV16 E7 M1 monoclonal antibody (Figure 1B). Recombinant and purified HPV16 E7 was used as a positive control, and this protein has a slower electrophoretic mobility than the E7 protein in cell extracts presumably due to the absence
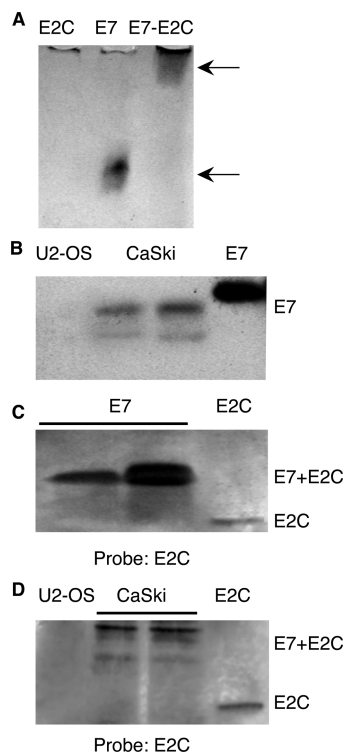
FIGURE 1: E2C−E7 interaction in native gel electrophoresis and a far Western assay. (A) E2C−E7 interaction analyzed by EMSA. In lane E2C, this protein does not appear in the native gel because of its high isoelectric point. In lane E7 and lane E2C-E7, the proteins are retarded compared to E7 alone. Arrows mark the positions of the E7−E2C complex and E7, respectively. (B) Detection of E7 in HPV-transformed cells by a Western blot. Different amounts of CasKi whole cell extracts (5 and 10 μg in lanes 2 and 3, respectively) and recombinant HPV16 E7 protein (10 ng in lane 4) were probed with the M1 monoclonal antibody. U2-OS whole cell extracts were used as a negative control (lane 1). (C and D) E2C−E7 interaction tested by far Western blotting. (C) Interaction between recombinant HPV16 E7 and E2C. Lanes 1 and 2 contained 5 and 10 ng of HPV16 E7, respectively. Lane 3 contained 5 ng of HPV16 E2C, used as a positive control. (D) Interaction between endogenous HPV16 E7 and recombinant HPV16 E2C. Lane 1 contained the U2-OS whole cell extract (negative control). Lanes 2 and 3 contained 5 and 10 μg of CaSki whole cell extracts, respectively. Lane 4 contained 5 ng of recombinant HPV16 E2C (positive control).

of post-translational modifications. As shown in the far Western assay using recombinant proteins (Figure 1C), the E2C probe specifically labeled the recombinant E7 band. The anti-E2C antibody used in these experiments did not cross react with purified E7 at concentrations 4-fold higher than those used in this experiment, validating its specificity in the far Western assay results (not shown). Despite its higher molecular mass (11 kDa) as compared to the E2C monomer (9.4 kDa), the migration of the E7 protein was retarded due to its anomalous electrophoretic mobility (13) The reciprocal far Western experiment (data not shown) showed that an E7 probe did not bind immobilized denatured E2C, suggesting that the direct protein−protein interaction requires a fully folded E2C. To determine whether the E2C probe can also bind to E7 from lysates of HPV-transformed cells, we repeated the far Western experiment. E2C bound to endogenous E7 from the CaSki cell line, while no binding was detected with the non-HPV-transformed cell line, U2-OS, confirming the specificity of E2C−E7 interaction (Figure 1D).

We next moved to solution binding experiments using highly purified recombinant E7 and E2C. Since preliminary experiments
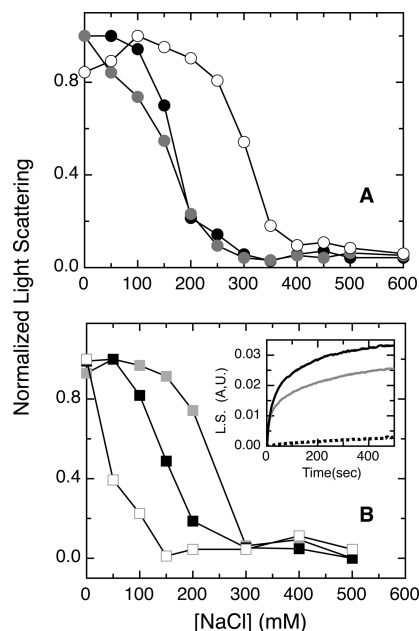

FIGURE 2: Characterization of E2C−E7 aggregation by light scattering. (A) E2C−E7 aggregation at pH 5.6 (○), 7.0 (gray circles), and 8.0 (●). In all cases, 4 μM E7 and 4 μM E2C were used in 25 mM Tris-HCl and 1 mM DTT. (B) E2C−E7 aggregation at different salt concentrations and different E7 states and domains: E7N (□), E7 (■), and E7SOs (gray squares). In all cases, 3 μM E7 and 3 μM E2C were used in the presence of 20 mM Tris-HCl (pH 8.0) and 1 mM DTT. The inset shows aggregation kinetics measured after both proteins had been mixed: E7N (···), E7 (—), and E7SOs (gray line). In all cases, 0.5 μM E7 conformers were incubated with 1 μM E2C in 20 mM Tris-HCl (pH 8.0) and 1 mM DTT without salt.

indicated a substantial tendency toward visible aggregation when both proteins were mixed, we analyzed the effect of ionic strength by increasing the buffer salt concentration and quantified aggregation by light scattering. Figure 2A shows that at 4 μM for each protein, the aggregation process is minimized at neutral pH (7.0−8.0) and 250 mM sodium chloride. At pH 5.6, higher salt concentrations are required to revert the aggregation, indicating a stronger tendency to precipitate at lower pHs.

As E7 protein can exist in different oligomeric species (14), and E7SOs were tested for aggregation. Given the highly acidic pI of E7 (4.2), the highly basic pI of E2C (9.8), and the influence of ionic strength on the interaction, we also tested the N-terminal acidic domain of E7, E7(1−40) (E7N), in the assay (19) as a likely binding determinant. While the complex with E7SOs displayed a salt-dependent aggregation similar to that of E7, those with E7-N exhibited a much weaker tendency to aggregate (Figure 2B). A similar conclusion can be drawn by following the aggregation process as a function of time using a lower concentration of each protein (0.5 μM), and without the addition of NaCl (Figure 2B, inset). This is indicative of soluble binding and constitutes the basis of the modular dissection described below.

It should be stressed that under the assay conditions used throughout this work, E2C is always a dimer (K_{dim} in the approximately picomolar range) (37), whereas E7 can present in a monomer−dimer equilibrium ($K_{dim} \sim 1 \mu$M) (38); we express its concentration as monomer.

Different E7−E2C Complexes Are Populated in Different Concentration Regimes. The nature and stoichiometry of the interaction and the aggregates formed were analyzed in a titration experiment at pH 8.0 in the absence of salt and monitored by light scattering, UV absorbance at 280 nm, and
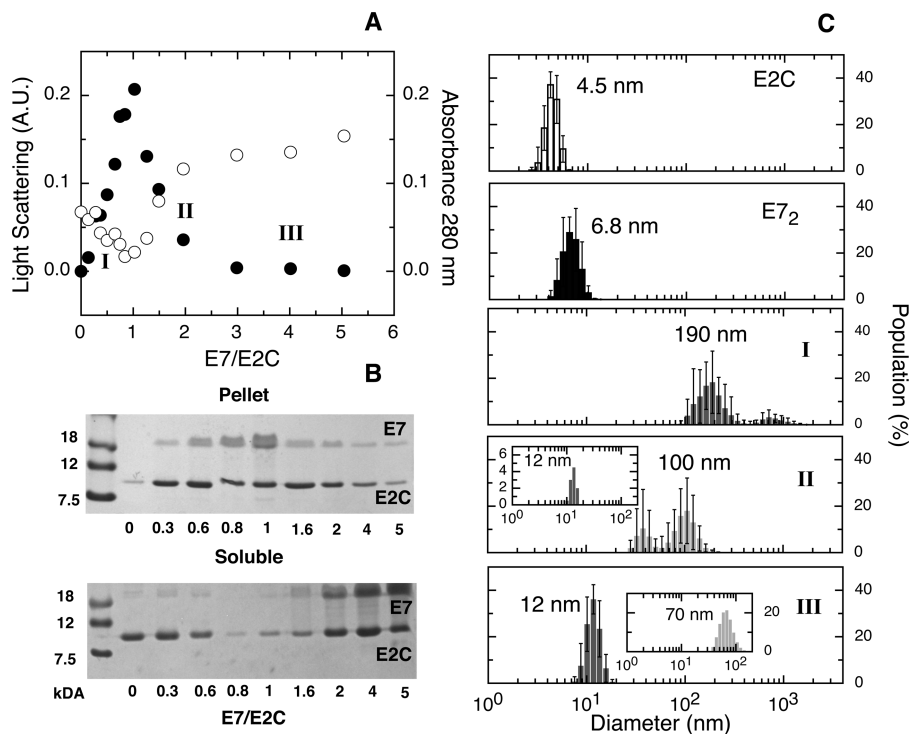
FIGURE 3: Behavior of E2C−E7 complexes at different relative concentrations of both proteins. (A) Measurements were taken in different tubes containing the same E2C concentration (2 μM) and varying E7 concentrations (see Experimental Procedures). We recorded the steady state scattering signal at 360 nm (●) and 280 nm absorbance (○) of the soluble fraction after centrifugation. (B) SDS−PAGE of the pellet fraction (top) and SDS−PAGE of the soluble fraction precipitated with TCA (bottom). (C) Size distribution measured by dynamic light scattering. The top panel shows the size distribution of 10 μM E2C, and the bottom panel corresponds to 10 μM E7. The other three panels correspond to three different conditions of the titration curves of panel A. (I) E2C in excess: 10 μM E2C and 4 μM E7. (II) E7:E2C ratio of approximately 2: 10 μM E7 and 4 μM E2C. (III) E7 in excess: 10 μM E7 and 3 μM E2C. The inset shows the particle distribution obtained by constraining the interval of analysis between 0.1 and 20 nm. All assays were performed with 20 mM Tris-HCl (pH 8.0) and 2 mM DTT.

SDS−PAGE. Increasing amounts of E7 were added to a fixed concentration of E2 in separate tubes, and measurements were taken once the steady state was reached (kinetic traces not shown). The light scattering signal reached a maximum at a an E7:E2C concentration ratio of 1 (Figure 3A). After this point, the signal decreases sharply at excess concentrations of E7, to reach a basal value (no aggregation) at a ratio of 2, equivalent to two E7 monomers per E2C dimer. After scattering measurements, each tube was centrifuged and the absorbance at 280 nm was determined in the supernatant. This signal corresponds mainly to E2C given the low molar extinction coefficient of E7 relative to that of E2C (6335 and 41940 $M^{-1} cm^{-1}$, respectively). A specular pattern was observed, i.e., minimal remainder concentration at maximum scattering. The basal slope with an excess of E7 corresponds to a linear increase with concentration due to the contribution from E7 tyrosines to absorbance.

The pellet and supernatant fractions from the assay described above were analyzed by SDS−PAGE. As the E7 concentration is increased up to a 1:1 molar ratio, the magnitudes of the bands corresponding to insoluble E2C and E7 increase (pellet fraction), whereas the magnitudes of the bands corresponding to soluble E2C (supernatant fraction) decrease. This behavior mirrors that seen in the light scattering assay, where the maximal visible aggregation was reached at a 1:1 stoichiometry. At a molar ratio of > 1:1, further increases in E7 concentration lead to a decrease in E2C and E7 concentrations in the pellet fraction, in parallel with an increase in E2C and E7 concentrations in the supernatant fraction. These assays confirm a dual behavior of these complexes, i.e., maximum aggregation at an E7:E2C concentration equal to 1, and maximum solubility of the complex in the

presence of an excess of E7 (Figure 3B). The solubility of E7 in the absence of E2C was assessed in the concentration range used in this experiment (0−12 μM), showing neither a detectable scattering signal nor an appreciable pellet after centrifugation (data not shown).

To further investigate the size and confirm the formation of the complexes, we made use of dynamic light scattering for measuring particle size. E2C yields a hydrodynamic diameter of 4.5 nm, in excellent agreement with the structure of the dimer (*39*), whereas E7 yields a hydrodynamic diameter of 6.8 nm, which shows twice its expected size (Figure 3C). This is in excellent agreement with previous results from our lab describing a dimeric extended conformation in solution (*13*). We next performed experiments in three different conditions from the titration curve shown in Figure 3A: (I) excess of E2C, (II) E7:E2C concentration ratio equal to 2, and (III) excess of E7. In an excess of E2, a visible white aggregate was observed with a diameter size of ∼1−2 μm (not shown). We refer to this species as insoluble aggregates (IA). After brief centrifugation, two particle populations are found, one with a hydrodynamic diameter of ∼190 nm and a broad and smaller population with a distribution near 1 μm (Figure 3C, I). These larger particles have a size to similar those found before centrifugation and should correspond to insoluble particles that remained in suspension. This heterogeneity is expected from the insoluble nature of the sample. When a ratio of 2 was assayed, two populations with particle sizes of ∼40 and ∼100 nm were observed (Figure 3C, II). We name all heterogeneous soluble species as E2C−E7 oligomers (E2E7Os). In an excess of E7, a well-defined narrow distribution with a hydrodynamic diameter of ∼12 nm is observed, and we name this species the E7−E2C

complex (E7E2Cx) (Figure 3C, III). In the last two assays, the samples present some large size particles that disappear after centrifugation, but these samples did not exhibit a visible white aggregate as in the case of an excess of E2C.

To find small amounts of particles that can be in equilibrium with the population presented before and that cannot be observed if the entire particle size range is considered, we performed data analysis by constraining the range to a specific zone (see Experimental Procedures). This analysis shows that a small population of particles with a hydrodynamic diameter of ~12 nm can be found for case (II), when the E7:E2C concentration ratio is approximately 2 (Figure 3C, II, inset). Following the same constrained analysis, a population with a hydrodynamic diameter of ~70 nm was found when there was an abundant amount of E7, case (III) (Figure 3C, III, inset).

Thus, there are three possible behaviors when these proteins interact. When the concentration of E2C is in excess, heterogeneous oligomers with a high hydrodynamic diameter appear, and they tend to leave the solution as IA. When the concentration of E7 increases, these oligomers, E2E7Os, are smaller and more soluble than in an excess of E2C. If the E7 concentration increases until exceeding twice the E2C concentration (that means one E2C dimer to two E7 monomers), we found E7E2Cx, soluble complexes with a defined size.

Finally, we performed far-UV CD spectroscopy to determine whether conformational changes in secondary structure take place in E7−E2C oligomers. We analyzed the maximum point of aggregation at an E7:E2C concentration ratio equal to 1 (IA) and in the minimum of scattering at an E7:E2C concentration ratio equal to 2 (E2E7Os). In both cases, the spectra of the mixture differ substantially from that of the sum of the individual proteins at the same concentration, indicating a conformational change due to interaction between both proteins (Figure 4). The CD spectra of each complex not only differ from the spectra of the individual components but also differ from each other, suggesting conformational differences among the different complexes. Differences in CD spectra intensity could be related to a sample lost due to aggregation, but the wavelength position of CD bands unequivocally confirms a conformational change. No further conclusions about this change can be drawn since one or both proteins may produce CD changes upon binding.

Mapping the Interaction Interface of the E2C−E7 Oligomer. A titration experiment was conducted with a fixed concentration of fluorescein-labeled E7 (FITC-E7) and increasing amounts of E2C. Changes in fluorescence anisotropy and light scattering were monitored in parallel. To reduce the level of aggregation, the experiment was conducted in a 100 mM NaCl buffer. However, both probes do not change in parallel; the scattering remains practically invariable until the E7:E2C concentration ratio is approximately 1.0 and then increases to reach a plateau at a 4-fold ratio. This suggests that a binding effect with a small anisotropy change is followed by a larger change due to oligomerization or aggregation, reported by both techniques. The dissociation constant for E7E2Cx cannot be accurately determined since the complex cannot be separated from E2E7Os or IA species under these conditions (Figure 5).

The ionic strength dependence of the process and the basic nature of E2C suggest that the acid N-terminal E7 domain could be involved in the interaction. To test this, we conducted an EMSA assay with HPV16 E7N and E2C. A band corresponding to the E2C−E7N complex becomes evident as the E2C concentration is increased (Figure 6A). An equimolar amount of E7C
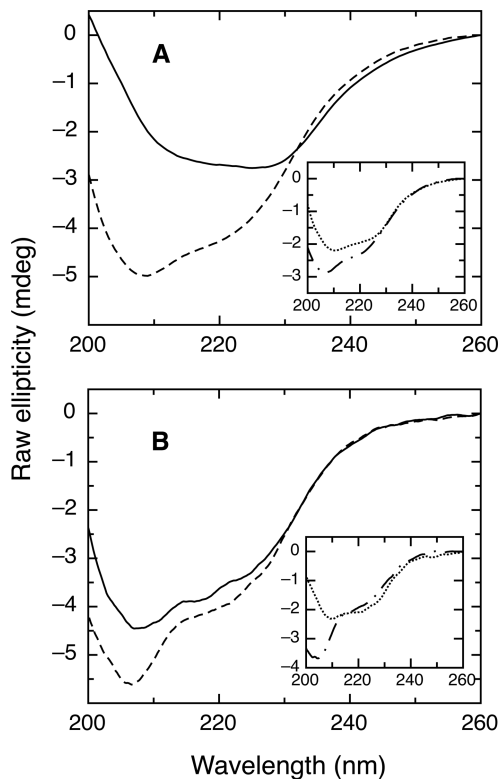

FIGURE 4: Far-UV CD spectra of different E7−E2C oligomers. (A) Spectrum of 2 μM E7 and 2 μM E2C. (B) Spectrum of 4 μM E7 and 2 μM E2C. Both assays were conducted in 20 mM Tris-HCl (pH 8.0) and 2 mM DTT. Mixtures of both proteins (—) and sum of E2C and E7 spectra (---). Insets shows E2C spectra (···) and E7 spectra (−·−).
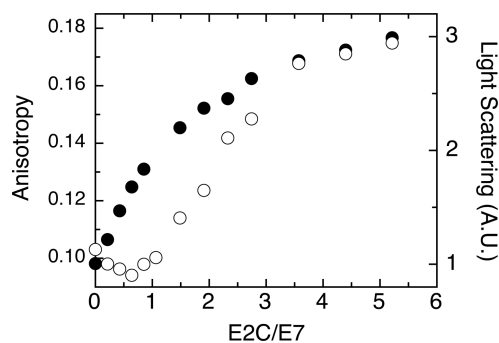

FIGURE 5: Fluorescence anisotropy and light scattering titrations of FITC-E7 with E2C. Titration of 200 nM FITC-E7 with increasing amount E2C in 20 mM Tris-HCl (pH 8.0), 100 nM NaCl, and 2 mM DTT. Anisotropy (●) and light scattering at 500 nm (○).

did not compete for the E7N−E2C interaction under identical native PAGE conditions (not shown), supporting the specificity of the E7N complex and implying that if E7C could interact with E2C, that interaction would be at least 1 order of magnitude weaker than the E7N−E2C interaction. As a control for the specificity of the interaction, a similar gel shift assay was performed using BVP1-E7N instead of HPV16 E7N. At 20 μM BPV1 E7N and 30 μM E2C, we observed no mobility shift in BPV1-E7N as compared to the bovine domain alone (data not shown).

As previously shown (Figure 2B), the E7N−E2C complex has a weaker tendency to aggregate, allowing the characterization of the process in solution. We conducted a binding experiment following the anisotropy change in FITC-E7N upon addition of
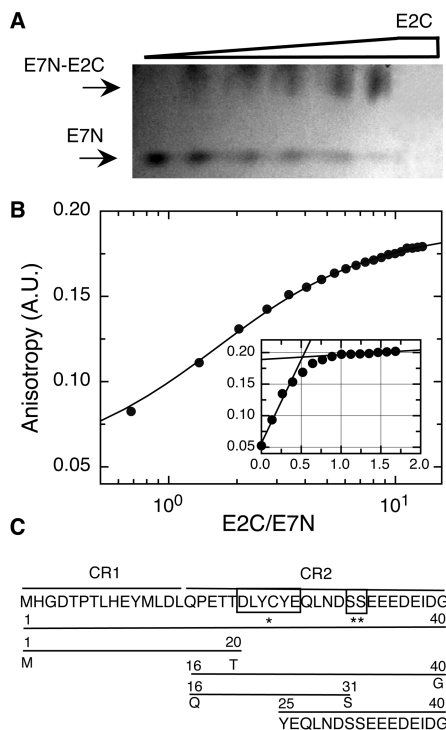
FIGURE 7: Displacement of E7-FITC and E7(1−40) from its complex with E2C by DNA followed by fluorescence anisotropy: FITC-E7 (●) and FITC-E7N (gray circles). The competition assays were performed via gradual addition of the competitive ligand (DNA duplex corresponding to E2 specific site 35) as the E2C−E7 complex or the E2C−E7N complex in 20 mM Tris (pH 8), 50 mM NaCl, and 2 mM DTT.

Table 2: Parameters for Binding of E7(1−40) to E2C DNA Binding Helix Mutants

	K_D (nM)	$\Delta\Delta G^a$ (kcal/mol)	$\Delta\Delta G_{E2C-DNA}{}^b$ (kcal/mol)
wild type	109 ± 28	0	0
K297A/Y301A	6098 ± 610	2.4 ± 0.2	2.9 ± 0.2
K297A	756 ± 76	1.1 ± 0.2	1.9 ± 0.1
K297R	52 ± 5	-0.4 ± 0.2	3.3 ± 0.1
Y301A	159 ± 20	0.2 ± 0.2	2.0 ± 0.1

[a]Obtained by subtracting the ΔG of wild-type E2C (9.4 kcal/mol). A positive value indicates weaker binding. [b]Taken from ref *41*.

change. In the absence of DNA, the interaction between either E7N or E7 and E2C is maximal as is the fluorescence anisotropy change (Figure 7). As the DNA concentration is increased, the complex is disrupted, reaching a basal value corresponding to free E7 (anisotropy change equal to zero). In other words, binding of DNA displaces E2C from the E7−E2C complex, indicating that the DNA binding helix of E2C is involved in the interaction. The comparison of both displacement curves shows that a larger amount of DNA is required to displace full-length E7 from the corresponding E2C complex than in the case of E7N, suggesting a tighter binding, not directly measurable because of solubility constraints (Figure 7).

Continuing with the same line of reasoning, and given the results described above, we considered the highly basic DNA binding helix as the candidate region for interaction with the acidic N-terminal domain of E7. We analyzed the binding of several site-directed mutants of the DNA binding helix to E7N in solution by fluorescence anisotropy. Results are listed in Table 2. Mutation of K297 to an alanine (K297A) decreases the affinity by 7-fold, with a free energy change, with respect to the wild type, of 1.2 kcal/mol. However, replacing the same residue with arginine (K297R) slightly stabilizes the binding. Mutating the noncharged contacting residue Y301 to alanine has a minimum effect on binding, while the double mutant K297A/Y301A causes destabilization of the complex. Upon application of the principles of double mutant cycles (*40, 41*), if the sum of the free energy changes of individual mutations is equal to that of the double mutant, the interaction is additive; if not, it is cooperative. In this case, there is a negative cooperativity of 1.1 kcal/mol [2.4 − (1.1 + 0.2) kcal/mol]; that is, the second mutation is more destabilizing than the sum of the individual replacements.

FIGURE 6: Mapping the binding region of E7. (A) Interaction of E7N with E2C in an electrophoretic mobility shift assay. E7N (20 μM) was incubated with increasing concentrations of E2C (0, 5, 10, 15, 20, and 30 μM). The last lane has E2C without E7N. E2C does not enter the native gel. Arrows mark the position of the E7N−E2C complex and E7N. (B) Titration of 100 nM FITC-E7N with E2C by fluorescence anisotropy. The binding constant (K_D) was calculated according to eq 1. The inset gives the binding stoichiometry: 1:2 E2C:E7N at 10 μM FITC-E7N. (C) N-Terminal region (CR1 and CR2) of E7 HPV16. One asterisk denotes the binding motif to pRB, and two asterisks denote serines that can be phosphorylated by casein kinase II. The lines below show all the peptides used. The E7(25−40) peptide, enriched with acid residues and containing a potential PEST sequence, is shown at the bottom. All E7 N-terminal peptides are labeled with FITC. The data for binding of E2C to peptides of the E7 N-terminus are listed in Table 1.

Table 1: Mapping the E2C Binding Region in the N-Terminal Domain of E7, E7N

peptide of E7	$K_D{}^a$ (nM)	$\Delta G_D{}^a$ (kcal/mol)
1−40	109 ± 28	9.4 ± 0.2
1−20	$> 2.3 \times 10^4$	< 6.3
16−40	203 ± 23	9.03 ± 0.07
16−31	$(6.3 \pm 0.4) \times 10^3$	7.02 ± 0.04
25−40	278 ± 20	8.85 ± 0.04

[a]Values obtained at 20 °C.

E2C (Figure 6B). The stoichiometry corresponds to one dimer of E2C per two molecules of E7N (Figure 6B, inset), and a K_D of 109 ± 28 nM was determined. To further map the interaction, we use a set of peptides described in Figure 6C. The K_D values for the different peptides assayed are listed in Table 1. An E7 peptide corresponding to amino acids 25−40 contains most of the binding energy for interacting with E2C (Figure 6C).

To determine whether E7 binding and DNA binding are competitive events, we preincubated 100 nM fluorescein-labeled E7N or full-length E7 with a 4-fold concentration of E2C. We subsequently added increasing amounts of a DNA duplex corresponding to the E2 specific site and measured the anisotropy
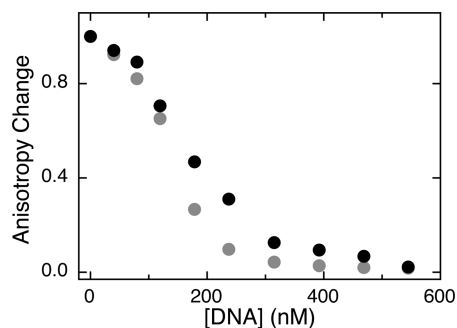
Finally, we considered the possibility that a peptide containing the entire DNA binding helix of E2 (α1-E2C) could interact with E7N. Using circular dichroism experiments and fluorescence anisotropy titrations of FITC-E7N, we found no evidence of interaction (not shown). This result indicates that the conformation of the binding helix given by the architecture, i.e., tertiary and quaternary structure of the full E2C domain, is required for binding E7 as in the case of E2C−DNA interaction (*42*).

DISCUSSION

Papillomaviruses have evolved to make use of complex yet efficient mechanisms for the utilization of the cell replication machinery through the control of the host cell cycle, a fact that ultimately allows PVs to replicate their genome and generate new infective particles (*43*). Focusing on this aspect of the viral biology, we find there are three proteins mainly involved: the two oncoproteins E6 and E7 that are directly involved in the control of host cell proliferation and the E2 transcription factor that regulates expression of these oncoproteins (*21, 44*). To generate a productive cycle, papillomaviruses require a stratified epithelium, from the basal cell layers, where the oncoproteins are actively expressed, to the external granular layers, where the late viral proteins are expressed and assembled into mature capsids. In this scenario, a host cell will change not only its intracellular milieu along the differentiation process, including factors such as the intracellular pH and redox potential, but also the levels of the viral proteins. Variation of protein expression across the stratified epithelium will cause the relative amount of each protein to change, allowing for different types of interactions between the viral proteins to occur. During this process, the E2 protein may regulate cell proliferation by direct interaction with E6 and E7 as well as by changing protein expression levels (*21, 31, 45*).

Both E2 and E7 make multiple interactions in cells, and both proteins can form oligomers in solution. These complexes may allow both proteins to form scaffolds that enable multiple partner proteins to interact and thereby integrate various signals. E2C is involved in oligomerization and aggregation during formation of a complex with specific DNA at low ionic strengths (*32*) and by mild modifications under the solvent conditions (*46*). These results, together with those from others (*47*), suggest that oligomerization might be a property inherent to E2C. The first evidence that allows us to conclude that these oligomerization properties could allow the formation of mixed heterogeneous oligomers comes from our data showing that E2C and E7 display a strong tendency to form insoluble aggregates (IA), which are largely dependent of ionic strength, indicative of an electrostatic nature. This is also true for the E7SOs, a spherical oligomeric species (*14, 15*), and to a much lesser extent E7N (*19*). The solubility of E7−E2 oligomers depends on pH, with a drastic change between pH 5.6 and 7.0, suggesting the involvement of histidine residues. Although we cannot rule out E7 histidines, the strong role of these groups in E2C folding, dynamics, DNA binding, and oligomerization (*46, 48−50*) suggests their participation in the process. This aggregation was observed even at the minimal concentration measurable (0.1 μM). Under these conditions, 85% of E7 will be monomeric according to its dissociation constant of 1 μM (*38*), indicating that dimerization is not required for the interaction. Separation of binding and aggregation processes by ionic strength modification was not possible for the full-length E7 protein, precluding an equilibrium measurement of the dissociation constant. Therefore, although not

quantifiable in solution, the irreversibility of the aggregate will cause its accumulation and would be expected to result in a similar effect in vivo (see below).

We describe three interaction regimes according to the relative concentration of the proteins. In an excess of E2C, there is a visible IA; in an excess of E7, the major species is the 12 nm diameter E7−E2C complex. At an E7:E2C concentration ratio approximately equal to 2, heterogeneous soluble E2E7Os species are observed, with a small population of the E7−E2C complex at excess E7, likely at equilibrium. This strongly suggests that a small excess of either of the molecules can shift the balance toward the large insoluble complexes or the defined soluble E7−E2C species and, therefore, establishes a highly sensitive mechanism that tunes the balance between the two proteins.

Our hypothesis that there is a connection between the electrostatic nature of the E2C−E7 interaction and the involvement of E7N and the basic DNA-binding site of E2C in the interaction was confirmed. The marked oligomerization−aggregation tendency observed and the different behavior of the full-length E7 could be due to a second weaker E2 binding site like that involving the C-terminal domain reported by others (*31*). Nevertheless, under our conditions, E7C does not interact at concentrations at which E7N is fully complexed by E2C. Mapping the sequences within E7N that are required to bind E2C shows that a peptide corresponding to amino acids 25−40 of E7 binds with a dissociation constant of 0.28 μM. Interestingly, this highly acidic region corresponds to the casein kinase II (CKII) phosphorylation site of HPV16 E7 (D30-S-S-E-E-E-D-E37). E2C appears to bind the E7 N-terminal domain at a different site used for Rb binding (L22-Y-C24-Y-E26), but even in the case in which binding of E2C would overlap with Rb, the 100-fold higher affinity of the latter for E7 will displace any E2C−E7 reversible interaction. However, a direct consequence of the E2C−E7 interaction has been observed in cells, that is, the stabilization of E7 protein by E2 (*31*). This could be the consequence of either blocking the PEST motif on HPV16 E7 protein which is contained within E7(25−40) (*19*) or sequestration of E7 in a more stable complex with E2. Although not specifically determined for E7, PEST motifs are often related to proteasome-mediated protein degradation in short-lived proteins with regions of extended structures such as E7 (*9*). An excess of E2 not only will sequester E7 but also has the potential of interfering with PEST-mediated degradation and could also modulate the degradation rate of E7. HPV16 E7N has a high (+8.7) PEST score in the same region where the CKII phosphorylation site is located, while BPV E7N displays a very low PEST score (−5.7) and does not bind HPV16 E2C (data not shown).

Evidence of the involvement of the DNA binding helix of E2C in the E7 interaction interface comes from displacement of E2C−E7 complexes by a specific E2 DNA site. Further, mutations in the E2 DNA binding helix have a direct impact on E7 N-terminal domain binding, and the change for a noncharged amino acid replacement, K297A or the double mutant K297A/Y301A, severely decreases affinity. It is worth mentioning that although DNA and E7 roughly share a binding region on E2C (the DNA binding helix), the natures of both interactions are different, as can be deduced from the fact that while E2 mutations on the DNA binding are additive, E2 mutations on E7 binding show a negative cooperativity of 1.1 kcal/mol. In addition, the change to the basic residue arginine (K297R) slightly increases the affinity for E7 ($\Delta\Delta G = -0.4$ kcal/mol), while a similar replacement causes a drastic destabilization of DNA binding

($\Delta\Delta G$ = 3.3 kcal/mol), due to steric hindrance caused by the bulkier guanidine group of arginine (*41*), which does not otherwise interfere with E7 binding. A peptide corresponding to the DNA binding helix of E2 does not bind E7, indicating that the interaction requires the positioning of this helix in a particular conformation in the context of the entire domain architecture, as was the case for the DNA interaction (*42*). This speaks of a level of specificity that cannot involve merely electrostatic forces. At this stage, we should state that our results concerning the interaction site do not match the results from protein truncation experiments using nonstructured fragments of E2 spanning part of the hinge domain and parts of the DNA binding domain, and these fused to GST (*31*). We believe that these differences may arise from the fact that dissecting a protein in domains or structural units will provide different information compared to gradual fragmentation based on amino acid sequence and as part of the same polypeptide as a tag protein such as GST (*31*). In fact, the absence of binding by the isolated DNA binding helix of E2 supports this.

We have previously shown that E7 can oligomerize into amyloid-like E7SOs and that these display chaperone holdase activity with standard nonrelated protein substrates (*14*, *15*). These oligomeric forms with amyloid-like properties accumulate in large excess in the cytosol exclusively, while monomeric−dimeric forms of E7 do so in the nucleus of several cell lines and carcinoma tissue; both species exist in a dynamic equilibrium (*16*). The fact that the N-terminal domain of E7 faces the solvent in E7SOs (*15*) agrees with our present observation of an interaction between E7SOs and E2C, and this needs further investigation. Hypothetically, if E2C is translated in the presence of high levels of cytosolic E7 oligomers, it is likely to be sequestered into hetero-oligomers, but we need to establish whether this leads to destabilization and degradation as one would assume. Thus, in the case of E2C, E7SOs could use their binding activity to take E2 out of solution rather than chaperoning it into soluble forms. The excess of free E7 protein may be readily degraded by the proteasome or be active in Rb binding and degradation. These interactions, and the fine-tuning exerted by changes in their levels along the infective cycle, would provide a tightly regulated mechanism for either controlling the transcriptional repression of oncogenes or degrading any excess of E7. In this way, adequate levels of E7 will be maintained, since uncontrolled transformation is detrimental for the virus life cycle as well as the host.

E2 and E7 come from the same viral genome and will share many features such as natural host cell, temporality of expression, localization and local concentration, regulation of their transcription by viral host cell elements, etc. These characteristics provide further support for the specificity of the interaction of these proteins, besides the submicromolar affinity. In addition, there are no E2 binding sites in the genome of an infected cell other than the four sites per HPV genome. This means that these sites can be saturated and interaction with E7 can still take place in the nucleus. Thus, E2 and E7 "see each other" in both cytosol and nucleus. As opposed to transfected species, endogenous E2 protein has been hardly detectable in cells, which means that its levels are strictly controlled along the infective cycle during epithelium differentiation, providing a plausible post-translational regulatory meaning for interaction with E7. A further regulatory step could be the fact that the E7 protein is a weak dimer, while E2 protein is an obligate dimer with subnanomolar dissociation constant under similar conditions (*37*). It is important to stress that the interaction we describe here is
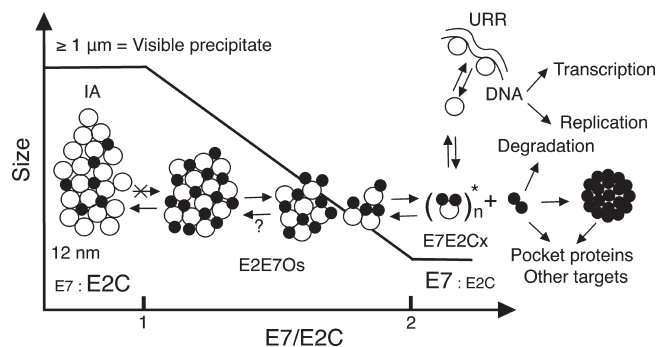

FIGURE 8: Model for the E2C−E7 interaction complexes. The figure shows the size distribution of the complexes as a function the E7:E2C concentration ratio. The distribution ranges from insoluble aggregates (IA) in an excess of E2C to heterogeneous oligomers (E7E2Os) and to the soluble complex (E7E2Cx) in an excess of E7. E2C dimers are represented in white and E7 monomers in black. The figure also shows the most representative cellular functions of E2C and E7 and how they may be regulated by an equilibrium between free proteins and the described complexes. An asterisk denotes E7E2Cx represented by its minimal formula, where the n subscript is a defined value between 1 and 5. The maximum value of n corresponds to the molecular weight for a globular protein of 12 nm and 223 kDa. This value could be smaller due to the fact that the E7 N-terminal domain is intrinsically disordered and noncompactly folded.

one of the two E7 interactions actually accurately quantified in solution using pure components; the other is the Rb tumor suppressor.

We propose the following hypothesis for the biological implications of the in vitro results we present here, summarized in Figure 8. As transcription of the viral early genes proceeds, the levels of both E2 and E7 proteins would increase gradually and E2 will repress transcription, keeping E7 level low. The cell differentiation process involves infected cells migrating to the upper layers of the epithelium with host cell factors affecting the translation−degradation balance of E2 and E7. An increase in the level of E7 expression causes entry into the S phase through targeting of Rb and other pocket proteins, although E7 levels are strictly controlled at a level that allows S phase entry, but not uncontrolled cell proliferation, something that would be detrimental for the virus life cycle. In this context, free E2 levels would start to decrease through direct interaction with E7. It is possible that newly synthesized E2 would then be retained in the cytosol where E7 is present as accumulations of oligomeric forms of the oncoprotein (*16*). This could prevent E2 from reaching the nucleus and, therefore, derepress the expression of E7 (and E6). The derepression of E7 is taken to the highest levels upon random viral integration and disruption of the E2 gene. We can conclude that the interaction between E2 and E7 can produce the relocalization of these proteins and regulate or modify their functions, in excellent agreement with recent results in cellular models (*30*). Further experiments are required to test the model proposed here, including the evaluation of the role of the E6−E2 interaction and the precise colocalization of E2, E7, and E6, and their relative protein levels in model cells and tissues. Finally, sequestering, insolubilization, or relocalization of E2 with excess E7 implies that the oncogene may also downregulate viral DNA replication by blocking access to the replication origin.

REFERENCES

1. zur Hausen, H. (2000) Papillomaviruses causing cancer: Evasion from host-cell control in early events in carcinogenesis. *J. Natl. Cancer Inst. 92*, 690–698.

2. World Health Organization (2007) Summary report on HPV and cervical cancer statistics in Argentina , HPV Information Center, Barcelona, Spain.

3. Frazer, I. (2002) Vaccines for papillomavirus infection. *Virus Res. 89*, 271–274.

4. Munger, K., Phelps, W. C., Bubb, V., Howley, P. M., and Schlegel, R. (1989) The E6 and E7 genes of the human papillomavirus type 16 together are necessary and sufficient for transformation of primary human keratinocytes. *J. Virol. 63*, 4417–4421.

5. Scheffner, M., Werness, B. A., Huibregtse, J. M., Levine, A. J., and Howley, P. M. (1990) The E6 oncoprotein encoded by human papillomavirus types 16 and 18 promotes the degradation of p53. *Cell 63*, 1129–1136.

6. Boyer, S. N., Wazer, D. E., and Band, V. (1996) E7 protein of human papilloma virus-16 induces degradation of retinoblastoma protein through the ubiquitin-proteasome pathway. *Cancer Res. 56*, 4620–4624.

7. Barbosa, M. S., Edmonds, C., Fisher, C., Schiller, J. T., Lowy, D. R., and Vousden, K. H. (1990) The region of the HPV E7 oncoprotein homologous to adenovirus E1a and Sv40 large T antigen contains separate domains for Rb binding and casein kinase II phosphorylation. *EMBO J. 9*, 153–160.

8. Ben-Saadon, R., Fajerman, I., Ziv, T., Hellman, U., Schwartz, A. L., and Ciechanover, A. (2004) The tumor suppressor protein p16-(INK4a) and the human papillomavirus oncoprotein-58 E7 are naturally occurring lysine-less proteins that are degraded by the ubiquitin system. Direct evidence for ubiquitination at the N-terminal residue. *J. Biol. Chem. 279*, 41414–41421.

9. Rechsteiner, M., and Rogers, S. W. (1996) PEST sequences and regulation by proteolysis. *Trends Biochem. Sci. 21*, 267–271.

10. Phelps, W. C., Munger, K., Yee, C. L., Barnes, J. A., and Howley, P. M. (1992) Structure-function analysis of the human papillomavirus type 16 E7 oncoprotein. *J. Virol. 66*, 2418–2427.

11. Lin, R., Beauparlant, P., Makris, C., Meloche, S., and Hiscott, J. (1996) Phosphorylation of IκBα in the C-terminal PEST domain by casein kinase II affects intrinsic protein stability. *Mol. Cell. Biol. 16*, 1401–1409.

12. Garcia-Alai, M. M., Gallo, M., Salame, M., Wetzler, D. E., McBride, A. A., Paci, M., Cicero, D. O., and de Prat-Gay, G. (2006) Molecular basis for phosphorylation-dependent, PEST-mediated protein turnover. *Structure 14*, 309–319.

13. Alonso, L. G., Garcia-Alai, M. M., Nadra, A. D., Lapena, A. N., Almeida, F. L., Gualfetti, P., and de Prat-Gay, G. (2002) High-risk (HPV16) human papillomavirus E7 oncoprotein is highly stable and extended, with conformational transitions that could explain its multiple cellular binding partners. *Biochemistry 41*, 10510–10518.

14. Alonso, L. G., Garcia-Alai, M. M., Smal, C., Centeno, J. M., Iacono, R., Castano, E., Gualfetti, P., and de Prat-Gay, G. (2004) The HPV16 E7 viral oncoprotein self-assembles into defined spherical oligomers. *Biochemistry 43*, 3310–3317.

15. Alonso, L. G., Smal, C., Garcia-Alai, M. M., Chemes, L., Salame, M., and de Prat-Gay, G. (2006) Chaperone holdase activity of human papillomavirus E7 oncoprotein. *Biochemistry 45*, 657–667.

16. Dantur, K., Alonso, L., Castano, E., Morelli, L., Centeno-Crowley, J. M., Vighi, S., and de Prat-Gay, G. (2009) Cytosolic accumulation of HPV16 E7 oligomers supports different transformation routes for the prototypic viral oncoprotein: The amyloid-cancer connection. *Int. J. Cancer 125*, 1902–1911.

17. Liu, X., Clements, A., Zhao, K., and Marmorstein, R. (2006) Structure of the human Papillomavirus E7 oncoprotein and its mechanism for inactivation of the retinoblastoma tumor suppressor. *J. Biol. Chem. 281*, 578–586.

18. Ohlenschlager, O., Seiboth, T., Zengerling, H., Briese, L., Marchanka, A., Ramachandran, R., Baum, M., Korbas, M., Meyer-Klaucke, W., Durst, M., and Gorlach, M. (2006) Solution structure of the partially folded high-risk human papilloma virus 45 oncoprotein E7. *Oncogene 25*, 5953–5959.

19. Garcia-Alai, M. M., Alonso, L. G., and de Prat-Gay, G. (2007) The N-terminal module of HPV16 E7 is an intrinsically disordered domain that confers conformational and recognition plasticity to the oncoprotein. *Biochemistry 46*, 10405–10412.

20. Thierry, F. (2009) Transcriptional regulation of the papillomavirus oncogenes by cellular and viral transcription factors in cervical carcinoma. *Virology 384*, 375–379.

21. Hamid, N. A., Brown, C., and Gaston, K. (2009) The regulation of cell proliferation by the papillomavirus early proteins. *Cell. Mol. Life Sci. 66*, 1700–1717.

22. Bechtold, V., Beard, P., and Raj, K. (2003) Human papillomavirus type 16 E2 protein has no effect on transcription from episomal viral DNA. *J. Virol. 77*, 2021–2028.

23. Wu, S. Y., Lee, A. Y., Hou, S. Y., Kemper, J. K., Erdjument-Bromage, H., Tempst, P., and Chiang, C. M. (2006) Brd4 links chromatin targeting to HPV transcriptional silencing. *Genes Dev. 20*, 2383–2396.

24. Poddar, A., Reed, S. C., McPhillips, M. G., Spindler, J. E., and McBride, A. A. (2009) The human papillomavirus type 8 E2 tethering protein targets the ribosomal DNA loci of host mitotic chromosomes. *J. Virol. 83*, 640–650.

25. Morgan, I. M., and Donaldson, M. M. (2006) The papillomavirus transcription/replication factor E2: Structure, function, cancer and therapy. In Papillomavirus Research: From Natural History to Vaccines and Beyond (Saveria Campo, M., Ed.) pp 73−82, Caisreir Academic Press, Wymondham, U.K.

26. Hegde, R. S. (2002) The papillomavirus E2 proteins: Structure, function, and biology. *Annu. Rev. Biophys. Biomol. Struct. 31*, 343–360.

27. Kalantari, M., Karlsen, F., Kristensen, G., Holm, R., Hagmar, B., and Johansson, B. (1998) Disruption of the E1 and E2 reading frames of HPV 16 in cervical carcinoma is associated with poor prognosis. *Int. J. Gynecol. Pathol. 17*, 146–153.

28. Graham, D. A., and Herrington, C. S. (2000) HPV-16 E2 gene disruption and sequence variation in CIN 3 lesions and invasive squamous cell carcinomas of the cervix: Relation to numerical chromosome abnormalities. *Mol. Pathol. 53*, 201–206.

29. Goodwin, E. C., Naeger, L. K., Breiding, D. E., Androphy, E. J., and DiMaio, D. (1998) Transactivation-competent bovine papillomavirus E2 protein is specifically required for efficient repression of human papillomavirus oncogene expression and for acute growth inhibition of cervical carcinoma cell lines. *J. Virol. 72*, 3925–3934.

30. Gammoh, N., Isaacson, E., Tomaic, V., Jackson, D. J., Doorbar, J., and Banks, L. (2009) Inhibition of HPV-16 E7 oncogenic activity by HPV-16 E2. *Oncogene 28*, 2299–2304.

31. Gammoh, N., Grm, H. S., Massimi, P., and Banks, L. (2006) Regulation of human papillomavirus type 16 E7 activity through direct protein interaction with the E2 transcriptional activator. *J. Virol. 80*, 1787–1797.

32. Ferreiro, D. U., Lima, L. M., Nadra, A. D., Alonso, L. G., Goldbaum, F. A., and de Prat-Gay, G. (2000) Distinctive cognate sequence discrimination, bound DNA conformation, and binding modes in the E2 C-terminal domains from prototype human and bovine papillomaviruses. *Biochemistry 39*, 14692–14701.

33. Pattillo, R. A., Hussa, R. O., Story, M. T., Ruckert, A. C., Shalaby, M. R., and Mattingly, R. F. (1977) Tumor antigen and human chorionic gonadotropin in CaSki cells: A new epidermoid cervical cancer cell line. *Science 196*, 1456–1458.

34. Cerutti, M. L., Centeno, J. M., de Prat-Gay, G., and Goldbaum, F. A. (2003) Antibody response to a viral transcriptional regulator. *FEBS Lett. 534*, 202–206.

35. de Prat-Gay, G., and Fersht, A. R. (1994) Generation of a family of protein fragments for structure-folding studies. 1. Folding complementation of two fragments of chymotrypsin inhibitor-2 formed by cleavage at its unique methionine residue. *Biochemistry 33*, 7957–7963.

36. Lakowicz, J. R. (1999) Principles of fluorescence spectroscopy , Plenum Press, New York.

37. Mok, Y. K., de Prat-Gay, G., Butler, P. J., and Bycroft, M. (1996) Equilibrium dissociation and unfolding of the dimeric human papillomavirus strain-16 E2 DNA-binding domain. *Protein Sci. 5*, 310–319.

38. Clements, A., Johnston, K., Mazzarelli, J. M., Ricciardi, R. P., and Marmorstein, R. (2000) Oligomerization properties of the viral oncoproteins adenovirus E1A and human papillomavirus E7 and their complexes with the retinoblastoma protein. *Biochemistry 39*, 16033–16045.

39. Hegde, R. S., Grossman, S. R., Laimins, L. A., and Sigler, P. B. (1992) Crystal structure at 1.7 Å of the bovine papillomavirus-1 E2 DNA-binding domain bound to its DNA target. *Nature 359*, 505–512.

40. Carter, P. J., Winter, G., Wilkinson, A. J., and Fersht, A. R. (1984) The use of double mutants to detect structural changes in the active site of the tyrosyl-tRNA synthetase (*Bacillus stearothermophilus*). *Cell 38*, 835–840.

41. Ferreiro, D. U., Dellarole, M., Nadra, A. D., and de Prat-Gay, G. (2005) Free energy contributions to direct readout of a DNA sequence. *J. Biol. Chem. 280*, 32480–32484.

42. Wetzler, D. E., Gallo, M., Melis, R., Eliseo, T., Nadra, A. D., Ferreiro, D. U., Paci, M., Sanchez, I. E., Cicero, D. O., and de Prat-Gay, G. (2009) A strained DNA binding helix is conserved for site recognition, folding nucleation, and conformational modulation. *Biopolymers 91*, 432–443.

43. Munger, K., Baldwin, A., Edwards, K. M., Hayakawa, H., Nguyen, C. L., Owens, M., Grace, M., and Huh, K. (2004) Mechanisms of human papillomavirus-induced oncogenesis. *J. Virol. 78*, 11451–11460.

44. de Prat-Gay, G., Gaston, K., and Cicero, D. O. (2008) The papillomavirus E2 DNA binding domain. *Front. Biosci. 13*, 6006–6021.

45. Grm, H. S., Massimi, P., Gammoh, N., and Banks, L. (2005) Cross-talk between the human papillomavirus E2 transcriptional activator and the E6 oncoprotein. *Oncogene 24*, 5149–5164.

46. Wetzler, D. E., Castano, E. M., and de Prat-Gay, G. (2007) A quasi-spontaneous amyloid route in a DNA binding gene regulatory domain: The papillomavirus HPV16 E2 protein. *Protein Sci. 16*, 744–754.

47. Sim, J., Ozgur, S., Lin, B. Y., Yu, J. H., Broker, T. R., Chow, L. T., and Griffith, J. (2008) Remodeling of the human papillomavirus type 11 replication origin into discrete nucleoprotein particles and looped structures by the E2 protein. *J. Mol. Biol. 375*, 1165–1177.

48. Mok, Y. K. (1996) Studies on the DNA binding domain from human papillomavirus strain 16 E2 protein, Ph.D. Thesis, University of Cambridge, Cambridge, U.K.

49. de Prat-Gay, G., Nadra, A. D., Corrales-Izquierdo, F. J., Alonso, L. G., Ferreiro, D. U., and Mok, Y. K. (2005) The folding mechanism of a dimeric β-barrel domain. *J. Mol. Biol. 351*, 672–682.

50. Eliseo, T., Sanchez, I. E., Nadra, A. D., Dellarole, M., Paci, M., de Prat-Gay, G., and Cicero, D. O. (2009) Indirect DNA readout on the protein side: Coupling between histidine protonation, global structural cooperativity, dynamics and DNA binding of the human papillomavirus type 16 E2C domain. *J. Mol. Biol. 388*, 327–344.